Periodic skyrmionic textures via conformal cartographic projections

David Marco, Isael Herrera, Sophie Brasselet, Miguel A Alonso

RESEARCH ARTICLE | NOVEMBER 04 2024

Periodic skyrmionic textures via conformal cartographic projections

Special Collection: Angular Momentum of Light

David Marco ; Isael Herrera ; Sophie Brasselet ; Miguel A. Alonso

APL Photonics 9, 110803 (2024)
https://doi.org/10.1063/5.0230959

Periodic skyrmionic textures via conformal cartographic projections

Cite as: APL Photon. 9, 110803 (2024); doi: 10.1063/5.0230959
Submitted: 27 July 2024 • Accepted: 21 October 2024 •
Published Online: 4 November 2024

David Marco,[1,2] Isael Herrera,[1] Sophie Brasselet,[1] and Miguel A. Alonso[1,3,4,5,a)]

AFFILIATIONS

[1] Aix Marseille Univ., CNRS, Centrale Med., Institut Fresnel, UMR 7249, 13397 Marseille Cedex 20, France
[2] Instituto de Bioingeniería, Universidad Miguel Hernández de Elche, 03202 Elche, Spain
[3] The Institute of Optics, University of Rochester, Rochester, New York 14627, USA
[4] Center for Coherence and Quantum Optics, University of Rochester, Rochester, New York 14627, USA
[5] Laboratory for Laser Energetics, University of Rochester, Rochester, New York 14627, USA

Note: This paper is part of the Special Topic on Angular Momentum of Light.
[a)] **Author to whom correspondence should be addressed:** miguel.alonso@fresnel.fr

ABSTRACT

We find periodic skyrmionic textures via conformal cartographic projections that map either an entire spherical parameter space or a hemisphere onto every regular polygon that provides regular tessellations of the plane. These textures minimize the energy inherent to the mapping and preserve the sign of the Skyrme density throughout the entire space. We show that 2D spinor fields (e.g., 2D polarization) that present periodic textures preserving the sign of the Skyrme density unavoidably exhibit zeros. We implement these textures in the polarization state of a laser beam.

I. INTRODUCTION

We refer to a 2D skyrmion as a distribution (or texture) over a plane of a vector field that completely spans a spherical parameter space while maintaining the sign of the Skyrme density ρ_S (the Jacobian between the sphere and the planar region occupied by the skyrmion). By definition, the Skyrme number, N_S, given by the integral of ρ_S over the region occupied by the skyrmion, is an integer. Merons are distributions that span one hemisphere, north or south; their Skyrme number is then $\pm 1/2$ when the hemisphere is spanned once.

The best-known examples of this type of texture are magnetic skyrmions,[1,2] which, due to their exceptional stability at nanoscale dimensions and low energy requirements for manipulation, are promising candidates for high-density, energy-efficient data storage technologies such as racetrack memory.[3] However, skyrmions and related 2D textures have been observed in a plethora of other physical systems, such as sound waves,[4,5] superfluids,[6,7] and optical fields.[8] In nonparaxial optical fields, isolated skyrmions whose vector parameter is the normalized photonic spin angular momentum[9,10] have been found. Periodic textures such as skyrmion lattices for the electric field's instantaneous orientation in evanescent waves[11] and spin optical meron lattices[12–16] have also been observed.

In paraxial optics, 2D skyrmionic textures in the polarization distribution over the transverse plane of monochromatic beams are often referred to as *Stokes textures*[8,17,18] since they span all normalized values of the Stokes vector, that is, the Poincaré sphere. Full Poincaré beams,[19–22] which display a spatially variant polarization pattern in a transverse section that is the stereographic projection of the Poincaré sphere, can be regarded as isolated skyrmions. While the motivation for studying optical skyrmions has perhaps been to find analogs of these interesting magnetic textures, these are likely to find applications for tailored light–matter interaction, such as creating spin textures in Bose–Einstein condensates.[23] Furthermore, the techniques used for generating them can lead to other applications. For example, the birefringent elements used for generating

Full Poincaré beams were later used in imaging polarimetry[24] and super-resolution fluorescence microscopy.[25]

Regarding periodic textures, optical polarization lattices of tiles that separately map each Poincaré hemisphere can be recognized as *Stokes meron lattices*. For example, the superposition of three plane waves with appropriate polarizations and wavevectors results in a triangular lattice.[26] In this lattice, ρ_S oscillates in sign, as does that in nonparaxial spin optical meron lattices.[12–15] This oscillation may lead to cancellation when integrating ρ_S, yielding $N_S \approx 0$ in some regions. In contrast, a few periodic textures turn out to avoid such cancellation since they preserve $\mathrm{sgn}(\rho_S)$ over all space, such as optical nonparaxial skyrmion lattices,[11] meron lattices in superfluid ^{3}He–A,[6] or textures in the velocity field of sound waves.[5] We recently proposed propagation-invariant optical polarization lattices that were designed to present this property.[27]

The first goal of this work is to study skyrmionic textures that preserve the sign of the Skyrme density. Such textures would result naturally from the accumulation of skyrmions with equal (nonzero) Skyrme numbers. We show that the subset of these textures for which the mapping from the sphere to the plane is conformal minimizes a geometric measure of the energy of the mapping. These textures are then stable when the interaction between skyrmions follows the minimization of this energy. As it turns out, the periodic conformal maps that describe these textures were developed in nineteenth- and twentieth-century cartography, where the sphere is mapped onto specific regular polygons. Physical space is then tessellated with these polygons without reflections, only translations and rotations. The spherical parameter space is then mapped as if it were the Earth [Fig. 1(a)].

Our second goal is the implementation of these conformal periodic skyrmion lattices as Stokes textures in paraxial monochromatic fields, for which the mapped spherical space is the Poincaré (or Bloch) sphere. We propose a prescription that generates well-behaved fields. We also find that the implementation of periodic skyrmionic structures with uniform $\mathrm{sgn}(\rho_S)$ necessarily implies that the field must present zeros, which makes the pattern sensitive to perturbations.

II. ENERGY MINIMIZATION

Consider the spherical parameter space spanned by the unit vector $\mathbf{s} = (\sin\theta\cos\phi,\ \sin\theta\sin\phi, \cos\theta)$. This sphere is then mapped onto the plane (x, y) as $\mathbf{s}(x, y)$. The Skyrme number, N_S, quantifies how many times this map wraps around the sphere (its sign giving the sense of wrapping) within a given planar region σ: $N_S = (4\pi)^{-1}\iint_\sigma \rho_S(x, y)\,dx\,dy$, where the Skyrme density $\rho_S(x, y)$ is defined as the Jacobian of the transformation, namely,

$$\rho_S(x, y) = \mathbf{s}(x, y)\cdot[\partial_x\mathbf{s}(x, y)\times\partial_y\mathbf{s}(x, y)]. \tag{1}$$

Let us first write the conditions for the map to be conformal. Infinitesimal changes of the same size in each of the two flat coordinates x, y must result in changes over the unit sphere of $\mathbf{s}$ also of equal size in two orthogonal directions. We can write this as

$$\mathbf{s}\times\partial_x\mathbf{s} = \mathrm{sgn}\,(\rho_S)\partial_y\mathbf{s}, \tag{2a}$$

$$\mathbf{s}\times\partial_y\mathbf{s} = -\,\mathrm{sgn}\,(\rho_S)\partial_x\mathbf{s}, \tag{2b}$$

where the operation $\mathbf{s}\times$ performs a rotation of 90° over the surface of the sphere. We can combine these equations as

$$\mathbf{s}\times\nabla\mathbf{s} = \mathrm{sgn}\,(\rho_S)\sigma_1\nabla\mathbf{s}, \qquad \sigma_1 = \begin{pmatrix} 0 & 1 \\ -1 & 0 \end{pmatrix}. \tag{3}$$

That is, a rotation over the sphere corresponds to a rotation over the plane. The equation above can also be written as

$$\nabla\mathbf{s} = -\,\mathrm{sgn}\,(\rho_S)\ \mathbf{s}\times(\sigma_1\nabla)\mathbf{s}, \tag{4}$$

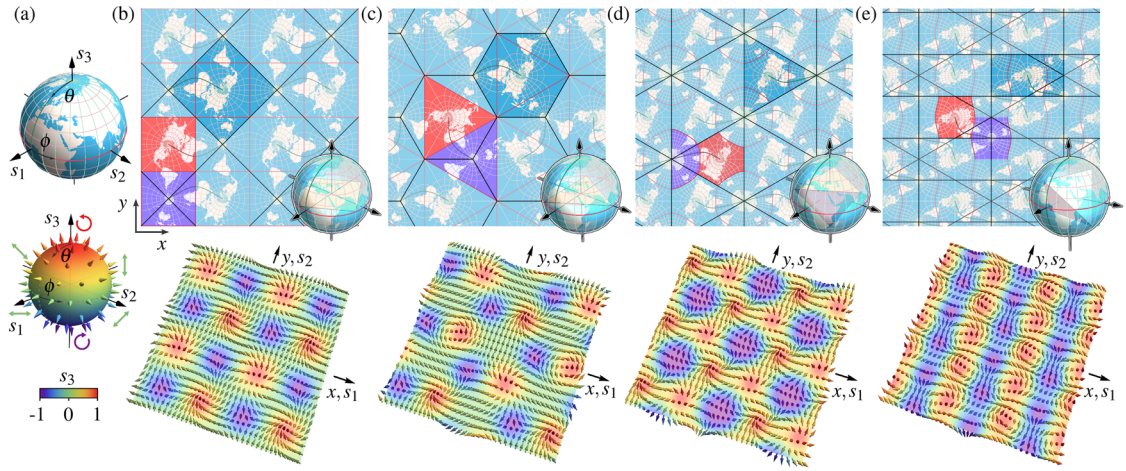

FIG. 1. (a) The Earth and a spanned spherical parameter space (e.g., the Poincaré sphere). (b)–(e) Periodic skyrmionic textures resulting from conformal cartographic mappings providing regular tessellations: (b) Peirce's quincuncial projection, (c) Adams' world in a hexagon, (d) Lee's world in a tetrahedron, and (e) Wray's variation of Lee's projection. For all, the entire sphere is mapped onto regular polygons (outlined in black), one of them highlighted in darker blue in each case. Rotated versions of these tessellate the plane. A northern and a southern hemisphere in each case are highlighted in red and purple, respectively.

where we must be careful distinguishing the vector operations in the two-dimensional flat space and the three-dimensional ambient space for **s** (in this case the cross product). It is easy to see that

$$\nabla^2\mathbf{s} = -\operatorname{sgn}(\rho_S)[(\nabla\mathbf{s})\times(\sigma_1\nabla\mathbf{s}) + \mathbf{s}\times(\nabla\sigma_1\nabla)\mathbf{s}] = \mathbf{0}. \quad (5)$$

The stretching of **s** over the plane can be considered as a local energy density given by the squared Euclidean norm of the 2×3 Jacobian matrix, that is

$$\varepsilon(x,y) = \frac{1}{2}\|\nabla\mathbf{s}\|^2 = \frac{1}{2}(\partial_i s_j)(\partial_i s_j), \quad (6)$$

where we used Einstein's convention of implicit summation over repeated indices, with $i = x, y$ and $j = 1, 2, 3$. The total energy over a unit cell σ is then given by $\mu = \iint_\sigma \varepsilon\, dxdy$. We now consider the functional derivative with respect to the function **s** of this energy. By using integration by parts to remove the derivatives of each factor of **s** and realizing that the integrated terms cancel due to the periodicity of the pattern, we arrive at

$$\frac{\delta}{\delta\mathbf{s}}\mu = -\nabla^2\mathbf{s}. \quad (7)$$

Equation (5) implies that this variation is then zero for a conformal distribution.

Note that for a conformal map, $\partial_x\mathbf{s}$ and $\partial_y\mathbf{s}$ have the same magnitude and are perpendicular, so the magnitude of the Skyrme density becomes

$$|\rho_S| = |\mathbf{s}\cdot\partial_x\mathbf{s}\times\partial_y\mathbf{s}| = |\partial_x\mathbf{s}||\partial_y\mathbf{s}| = \frac{|\partial_x\mathbf{s}|^2 + |\partial_y\mathbf{s}|^2}{2} = \varepsilon. \quad (8)$$

Thus, for all conformal maps, $\mu = 4\pi|N_S|$, and more generally, the total energy over a unit cell of any periodic texture with constant $\operatorname{sgn}(\rho_S)$ has a minimum value of $4\pi|N_S|$, this minimum being achieved for conformal maps.

III. CARTOGRAPHIC MAPPINGS

We now present the conformal cartographic transformations and their implementation as skyrmionic textures (Fig. 1). Only three tiles provide regular tessellations:[28] squares, equilateral triangles, and regular hexagons. We explore conformal maps that yield regular tessellations where either the entire sphere or a hemisphere is mapped onto each regular polygon. The only case left out is that where a hemisphere is mapped onto a hexagon, since it is impossible to tile the plane without edge conflicts using only rotated copies of hexagonal merons (that is, one could not avoid having two hexagons mapping the same hemisphere sharing a side).

We begin with Peirce's *quincuncial* projection,[29] which maps the whole sphere and also each hemisphere onto a square. The vertices of each square tile mapping a hemisphere are equally spaced along the sphere's equator [Fig. 1(b)]. The map is conformal except at these four points. The resulting meron texture is topologically equivalent and morphologically similar to a texture resulting from energy minimization in superfluid ^{3}He–A.[6]

We consider Adams' *world in a hexagon* projection,[30] which maps the sphere onto a regular hexagon while mapping each hemisphere onto an equilateral triangle. This map exhibits singular points at the vertices of each triangular tile that spans a hemisphere, which is again equally spaced along the equator [Fig. 1(c)]. We recently generated a Stokes texture corresponding to the superposition of a few plane waves that is topologically equivalent to this map, although not conformal.[27]

Finally, we explore a map of the entire sphere onto an equilateral triangle, known as Lee's *world in a tetrahedron* projection.[31] Here, the sphere is divided into four equal spherical equilateral triangles, each being then projected onto the corresponding face of a regular tetrahedron. Unfolding the tetrahedron yields an equilateral triangle that tessellates the plane with rotated copies of itself. Note that one of the tetrahedron's vertices is chosen to be at the south pole [Fig. 1(d)]. This texture is topologically equivalent and morphologically similar to one generated recently in the instantaneous velocity field of sound waves.[5] Wray proposed a modified version of Lee's mapping[32] where the two poles are positioned at the midpoints of two opposing edges of the tetrahedron [Fig. 1(e)]. Unlike Lee's original projection, in Wray's transformation, the equator does not form closed loops but meandering lines. Upon unfolding the tetrahedron, the resulting triangle can be rearranged as a rectangle (with aspect ratio $\sqrt{3}:1$), yielding a tessellation of rectangles. In both versions of Lee's projection [Figs. 1(d) and 1(e)], the singular points are placed at the vertices of the tetrahedron.

These maps can be expressed as a sequence of two conformal transformations: a planar map defined by an analytic function $w(z)$, where $z = x + iy$ (x and y being the Cartesian coordinates in physical space), and a stereographic projection from the north pole. These operations result in a map from the plane to the sphere's azimuthal and polar coordinates as $\phi = \arg[w(z)]$ and $\theta = 2\arctan|w(z)|$, respectively.

For Peirce's and Adams' projections, $w(z)$ is the inverse function of the Schwarz–Christoffel transformation[33] that maps the unit disk onto a square[34] and an equilateral triangle,[32] respectively. The expressions for $w(z)$ for each of these projections (Peirce[34], Adams, Lee, and Wray[32]) are as follows:

$$w_P(z) = \frac{e^{i(\phi_0+\alpha)}}{\sqrt{2}}\operatorname{sd}\left(\tilde{z}_1, \frac{1}{\sqrt{2}}\right), \quad (9a)$$

$$w_A(z) = e^{i(\phi_0+\alpha)}\operatorname{sm}(\tilde{z}_2), \quad (9b)$$

$$w_L(z) = 2^{1/6}e^{i(\phi_0+\alpha)}\operatorname{sm}(\tilde{z}_2)\operatorname{cm}(\tilde{z}_2), \quad (9c)$$

$$w_W(z) = \frac{e^{i(\phi_0+\alpha)}}{2}\operatorname{sd}\left(\tilde{z}_3, \frac{\sqrt{3}-1}{2\sqrt{2}}\right), \quad (9d)$$

where sd is the ratio between the Jacobi elliptic functions sn and dn, while sm and cm correspond to the Dixon elliptic functions, which can be expressed in terms of the Weierstrass elliptic function denoted as $\wp(z)$ and its derivative $\wp'(z)$: $\operatorname{sm}(z) = 6\wp(z)/(1 - 3\wp'(z))$ and $\operatorname{cm}(z) = (3\wp'(z) + 1)/(3\wp'(z) - 1)$.[35] The three complex numbers $\tilde{z}_i$ are defined as $\tilde{z}_{1,2,3} = \gamma_{1,2,3}\, e^{-i\alpha}(z - z_0)/d$, with $\gamma_1 = \Gamma^2(1/4)/(2\sqrt{2\pi})$, $\gamma_2 = \Gamma^3(1/3)/(2\pi)$, and $\gamma_3 = 3^{1/4}\Gamma^3(1/3)/(2^{1/3}\pi)$, where Γ denotes the gamma function. The angle α rotates the polygon onto which the sphere is mapped, while ϕ_0 sets the initial value from which ϕ is swept within this polygon. Note that ϕ_0 influences

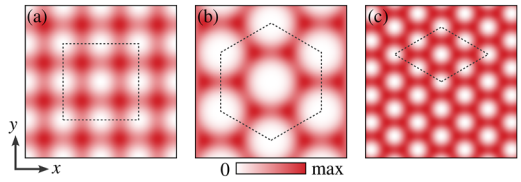

FIG. 2. Skyrme density for (a) Peirce, (b) Adams, and (c) Lee/Wray maps within the area displayed in Fig. 1. The unit cell of each texture is outlined by dashed lines.

the type of meron that appears in the textures (e.g., Néel- or Bloch-type[8]). The real and imaginary parts of the complex number z_0 are the x and y coordinates defining the center of the map. Finally, d sets the length of the edge of either the square or the equilateral triangle spanning a hemisphere in the case of Peirce's and Adams' mappings, while for Lee's and Wray's mappings, it corresponds to the length of the edge of the triangle spanning the sphere. Note that, due to the periodicity of the Jacobi and Dixon elliptic functions, these mappings work over the whole plane and not only within a central tile. The periodicity of the tiling is then natural. The inverse transformations to each of the mappings in Eq. (9) are given in Sec. I of the supplementary material.

The Skyrme number can be expressed as $\rho_S = \rho_{SP}\rho_w$, where $\rho_{SP} = 4(1+|w(z)|^2)^{-2}$ is the Jacobian of the stereographic projection, and $\rho_w = [\partial_x \mathrm{Re}(w(z))]^2 + [\partial_y \mathrm{Re}(w(z))]^2$ is that for the transformation $w(z)$ (simplified by using the Cauchy–Riemann conditions). These equations imply that ρ_S is always positive, as shown in Fig. 2. Within the context of cartography, this means that the shapes of the continents are never reversed. A different convention for the stereographic projection could be used that reverses its sign, leading to textures with $\mathrm{sgn}(\rho_S) < 0$.

Note that $N_S = 1$ within the polygons that map the entire sphere for all projections in Fig. 1. Peirce's and Adams' projections lead to lattices of square and triangular merons, respectively, in which any two neighboring merons map different hemispheres. Within each meron, $N_S = 1/2$. Nevertheless, in the first version of Lee's projection [Fig. 1(d)], there are merons that span twice the southern hemisphere, leading to $N_S = 1$. In fact, both in Lee's and Wray's versions of the tetrahedron projection, different regions covering the same hemisphere are in direct contact and not separated by a line corresponding to the equator, so these textures do not classify as meron lattices according to some definitions.[1]

IV. PERIODIC SKYRMIONIC TEXTURES IN MONOCHROMATIC PARAXIAL OPTICAL FIELDS

We now explore the implementation of these skyrmionic textures in the spatial distribution of polarization for a monochromatic optical beam of frequency ω. The instantaneous transverse real electric field at any point (x,y) and time t is given by $\boldsymbol{\mathcal{E}} = \mathrm{Re}[\mathbf{E}\exp(-i\omega t)]$, where $\mathbf{E}$ is the complex field, which can be parameterized as

$$\mathbf{E} = E_0\left[\cos(\theta/2)\mathbf{l} + e^{i\phi}\sin(\theta/2)\mathbf{r}\right] = E_\mathbf{l}\mathbf{l} + E_\mathbf{r}\mathbf{r}, \tag{10}$$

with E_0 being a complex function of x and y that provides an overall amplitude and phase and that does not affect the polarization (defined by the expression in brackets). Here, the unit vectors $\mathbf{l},\mathbf{r} = (\mathbf{x} \pm i\mathbf{y})/\sqrt{2}$ represent left- and right-circular polarization, where $\mathbf{x}$ and $\mathbf{y}$ are the unit vectors along the x and y axes, respectively. The circular polarization components $E_{\mathbf{l},\mathbf{r}}$ are the complex functions of x and y, whose relative phase is $\phi = \phi_\mathbf{r} - \phi_\mathbf{l}$ (with $\phi_{\mathbf{r},\mathbf{l}} = \arg[E_{\mathbf{r},\mathbf{l}}]$). At each point, $\boldsymbol{\mathcal{E}}$ traces over each optical cycle an ellipse within the transverse plane, whose ellipticity and handedness are determined by θ, while ϕ gives twice the orientation angle of its major axis with respect to x. Each possible polarization ellipse then corresponds to a point on the Poincaré sphere [Fig. 1(a)] described by a normalized Stokes vector $\mathbf{s} = (\sin\theta\cos\phi,\ \sin\theta\sin\phi, \cos\theta)$. Spanning the Poincaré sphere then means achieving every paraxial polarization. The northern and southern hemispheres correspond to left- and right-handed ellipses, respectively, with the two poles corresponding to the two circular polarizations, while linearly polarized ellipses are positioned along the equator.

We now find equations for optical fields that implement these textures independently of the mapping function $w(z)$. Since $w(z) = \tan(\theta/2)e^{i\phi}$, $\mathbf{E} = E_\mathbf{l}(z)[\mathbf{l} + w(z)\mathbf{r}]$, any reasonable choice for $E_\mathbf{l}(z)$ leads to the desired polarization texture as long as $E_\mathbf{r}(z) = E_\mathbf{l}(z)w(z)$. However, it is convenient to choose a functional form that avoids singularities in the field and that treats the two hemispheres similarly. In our convention, the hemisphere with left(right)-handed ellipses corresponds to $|w(z)| < (>)1$, with the pole representing left(right)-circular polarization corresponding to $w(z) = 0$ (∞). It is then desirable to find an expression for $E_\mathbf{l}(z)$ such that $E_\mathbf{r}(z) = E_\mathbf{l}(z)w(z)$ takes a similar functional form except for the replacement $w \to w^{-1}$. One such solution is

$$E_{\mathbf{l},\mathbf{r}}(z) = A\sqrt{-w_0^{\pm 1}}\,\frac{[w^{\pm 1}(z) - w_0^{\pm 1}]^*}{|w^{\pm 1}(z)|^2 + |w_0^{\pm 1}|^2}, \tag{11}$$

where A is a constant amplitude factor and w_0 is a dimensionless constant. Note that both polarization components vanish at points where $w(z) = w_0$, meaning that this construction forces zeros in the field at points where the polarization is such that $\tan(\theta/2)e^{i\phi} = w_0$. As we discuss later, this feature has a topological origin. In what follows, we choose $w_0 = -1$ to simplify the expressions so that the zeros coincide with points of vertical linear polarization.

We now focus on Peirce's texture as a representative example, for which Fig. 3 shows the intensity and phase of $E_{\mathbf{l},\mathbf{r}}$ (a), as well as the polarization and intensity distributions (b). The figures for the other maps are shown in Sec. II of the supplementary material, which also includes plots of the fields' discrete Fourier spectra for the four maps.

These textures correspond to optical polarization lattices[36] exhibiting polarization singularities such as L-lines (lines of linear polarization) and C-points (points of circular polarization).[37] C-points emerge in regions where a vortex in $\phi_{\mathbf{l},\mathbf{r}}$ with topological charge $m_{\mathbf{l},\mathbf{r}}$ is superimposed onto a region with no vortex in $\phi_{\mathbf{r},\mathbf{l}}$, rendering a vortex in ϕ with topological charge $m_\phi = \mp m_{\mathbf{l},\mathbf{r}}$. The polarization ellipse undergoes a rotation of $m_\phi\pi$ radians around the singularity in ϕ. For $m_\phi > 0$, the ellipse performs a counterclockwise rotation, while for $m_\phi < 0$ it rotates clockwise. In the proximity of C-points with $m_\phi = \pm 1$, the ellipses exhibit distinct singular patterns known as lemons $(m_\phi = 1)$ and stars $(m_\phi = -1)$.[37]

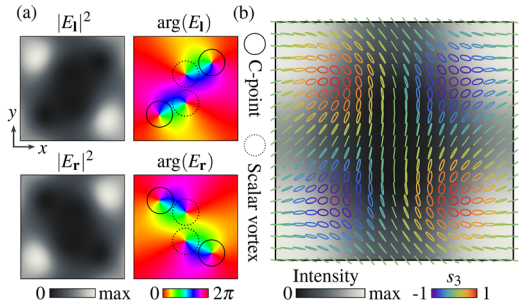

FIG. 3. Unit cell of the beam implementing in its polarization state Peirce's texture according to Eq. (9) with $\alpha = \pi/4$, $\phi_0 = 7\pi/6$, and $z_0 = (-1+i)/2$. (a) Theoretical intensity and phase distributions of the circular polarization components $E_{l,r}$. (b) Polarization and intensity distributions. Phase vortices result in either C-points or scalar vortices.

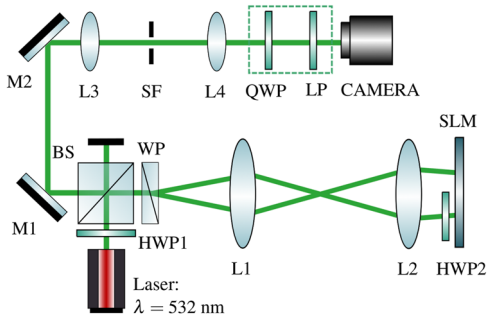

FIG. 4. Scheme of the experimental setup. Half-wave plate (HWP), beam splitter (BS), Wollaston prism (WP), lens (L), spatial light modulator (SLM), spatial filter (SF), quarter-wave plate (QWP), linear polarizer (LP), and mirror (M).

The polarization distribution in Fig. 3(b) shows an important feature: For a texture where $\rho_S > 0$ everywhere, all left(right)-handed C-points originate from a ϕ vortex with $m_\phi > (<)0$, and then all C-points with $m_\phi = \pm 1$ manifest as left-handed lemons and right-handed stars. (For a texture where $\rho_S < 0$ everywhere, the situation would reverse.) A way to understand this fact comes from considering mapping a small patch of the sphere. Let the polar coordinates of the local planar map be (r, φ). When mapping the north pole, $r \approx \kappa\theta, \varphi = \phi$, where κ is a positive constant. The Skyrme density has the same sign as the Jacobian between (θ, ϕ) and (r, φ), which equals $1/\kappa > 0$. Now consider transporting continuously the map to the south pole without reversing local directions (i.e., ρ_S does not change sign). At the south pole, the coordinates can be set to $r \approx \kappa(\pi - \theta), \varphi = -\phi$, which yield the same positive Jacobian. However, $m_\phi = \partial_\varphi \phi$ is positive at the north pole (left-circular polarization) and negative at the south pole (right-circular polarization).

Together with a well-established result from index theory, this result implies that paraxial fields displaying periodic skyrmionic Stokes textures that maintain $\mathrm{sgn}(\rho_S)$ must inevitably present zeros. This is because, within a unit cell of a periodic complex scalar field, the topological charges of its vortices must add up to zero. However, as just discussed, the vortices for each circular component that leads to C-points all have the same charge. Each component must then include extra vortices with the opposite charge, and the only way for these not to produce extra C-points is if their locations coincide for the two circular components, hence giving rise to field zeros. The field construction in Eq. (11) naturally introduces these zeros, placing them at points with a specific polarization.

It is important to emphasize that the presence of zeros for textures that maintain $\mathrm{sgn}(\rho_S)$ extends beyond textures implemented in paraxial polarization; it applies to any texture in a 2D spinor field achieved through the factorization of a global phase and amplitude function in a 2D complex vector field. Consequently, in such fields, a periodic texture that preserves $\mathrm{sgn}(\rho_S)$ inevitably presents zeros.

V. EXPERIMENTAL SETUP AND RESULTS

We experimentally generate the textures by implementing the circular polarization distributions from Eq. (11) in a continuous-wave laser beam using a spatial light modulator (SLM),[38] as shown in Fig. 4. The laser's polarization is controlled by a half-wave plate (HWP1) before entering a beam splitter (BS) and a Wollaston prism (WP), which splits the linear polarization components. A telescopic system magnifies these components onto the SLM. The beams are modulated using an algorithm that enables both amplitude and phase modulation with a phase-only SLM.[39] (Instead of directly modulating the circular polarization components, we modulate the horizontally and vertically polarized components, which can be easily expressed in terms of the circular ones.)

A second half-wave plate (HWP2) is placed in one arm before the SLM to align the polarization along the direction modulated by the SLM. After reflection on the SLM, HWP2 restores the arm's original polarization state, allowing the beams to be recombined after the WP. The recombined beams then travel through the BS to a second telescopic system, which images the SLM plane onto a CMOS camera. The field's polarization distribution is analyzed using a linear polarizer (LP) and a quarter-wave plate (QWP). The measured intensities of various polarization projections are used to compute the skyrmionic texture. More experimental details and data processing steps are provided in Sec. III of the supplementary material.

Figure 5 shows, for Peirce's projection, the measured Stokes vector distribution (a) and ρ_S (b). Similar results for the other three projections are given in Sec. IV of the supplementary material. For all cases, small regions of highly negative ρ_S emerge near the points where Eq. (11) predicts the field's zeros (corresponding to vertical polarization). This is because these zeros are unstable: any small relative misalignment of the polarization components causes the

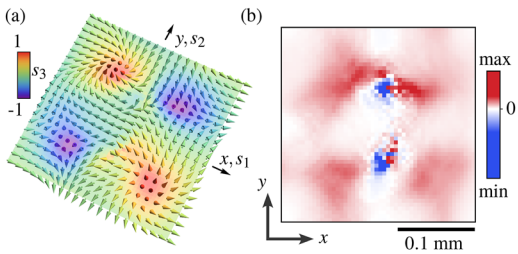

FIG. 5. Unit cell of the measured (a) Stokes vector distribution and (b) Skyrme density for Peirce's field.

intensity not to vanish exactly and the polarization to vary rapidly, covering within a small region the entire sphere in the opposite sense. Possible experimental sources of zero misalignment are defocus or the clipping of diffraction orders by the aperture. Excluding some orders carrying low intensities has little effect on the overall pattern but leads to rapid polarization variation in low-intensity regions (see Sec. V of the supplementary material), similar to that in the measured data.

VI. CONCLUSIONS

The skyrmionic lattices presented here represent different morphologies and topologies that preserve $\mathrm{sgn}(\rho_S)$. The fact that they are conformal implies that they minimize the energy inherent to the mapping. Note that rotated versions (in the spherical space) of each of these cartographic maps can also be considered, such as the two forms of Lee's projection. Similarly, some of these maps accept deformations while still tessellating the plane but not with regular polygons, and perhaps not conformally. It is possible, for example, to deform continuously Wray's map by transporting the singular points along meridians to the equator, arriving at a rotated version of Peirce's map. This means that Lee's, Wray's and Peirce's maps are topologically equivalent. Note, however, that changing the spacing of the singular points in Peirce's map until two of them merge would not lead to Adams' map (and would not be consistent with tessellation of the plane), meaning that this latter map (with three singular points) is topologically different from the others (with four singular points).

Other conformal projections that tessellate the plane can also be explored,[32,34] such as maps of the sphere onto a triangle or a square using Lagrange's projection of the sphere onto a disk[40] instead of the stereographic projection. An interesting case is Adams' *world in a square* projection,[41] which renders merons spanning a hemisphere four times for both hemispheres. Another texture with merons spanning a hemisphere six times for one of the hemispheres results from Cox's *world in a triangle* projection.[42]

For polarization textures (or any spinor field resulting from a 2D complex vector field), achieving uniform $\mathrm{sgn}(\rho_S)$ requires zeros in the vector field, making the texture unstable to perturbations, although instability under propagation can be reduced in some cases.[27] Exploring the inevitable occurrence of zeros in spinor fields beyond optics, such as Bose–Einstein condensates,[23] opens up an area for further investigation.

Finally, it would be interesting to study if periodic textures with uniform $\mathrm{sgn}(\rho_S)$, conformal or not, exist for higher dimensionalities. Recently, optical implementations of skyrmionic structures spanning three-spheres[43,44] and four-spheres[45] were proposed, the latter corresponding to a space–time periodic texture spanning all states of monochromatic nonparaxial polarization but with nonuniform $\mathrm{sgn}(\rho_S)$.

SUPPLEMENTARY MATERIAL

The supplementary material covers the inverse transformations of the mappings, theoretical and measured distributions for Adams, Lee, and Wray textures, spectra of the fields, experimental implementation, and the effects of clipping low-intensity diffraction orders by the aperture.

ACKNOWLEDGMENTS

This research received funding from the Agence Nationale de Recherche (ANR) through Project 3DPol, ANR-21-CE24-0014-01. D.M. acknowledges the Ministerio de Universidades, Spain, Universidad Miguel Hernández, and the European Union (Next Generation EU Fund) for a Margarita Salas grant from the program Ayudas para la Recualificación del Sistema Universitario Español and funding from the Ministerio de Ciencia e Innovación, Spain, Grant No. PID2021-126509OB-C22.

AUTHOR DECLARATIONS

Conflict of Interest

The authors have no conflicts to disclose.

Author Contributions

David Marco: Conceptualization (equal); Data curation (equal); Formal analysis (equal); Funding acquisition (equal); Investigation (equal); Visualization (equal); Writing – original draft (equal); Writing – review & editing (equal). **Isael Herrera**: Conceptualization (supporting); Data curation (lead); Investigation (equal); Validation (lead); Visualization (supporting); Writing – original draft (supporting); Writing – review & editing (equal). **Sophie Brasselet**: Conceptualization (equal); Funding acquisition (equal); Investigation (equal); Supervision (equal); Writing – original draft (equal); Writing – review & editing (equal). **Miguel A. Alonso**: Conceptualization (equal); Formal analysis (equal); Funding acquisition (equal); Investigation (equal); Supervision (equal); Writing – original draft (equal); Writing – review & editing (equal).

DATA AVAILABILITY

The data that support the findings of this study are available from the corresponding author upon reasonable request.

REFERENCES

[1] N. Nagaosa and Y. Tokura, "Topological properties and dynamics of magnetic skyrmions," Nat. Nanotechnol. **8**, 899–911 (2013).
[2] X. Yu, W. Koshibae, Y. Tokunaga, K. Shibata, Y. Taguchi, N. Nagaosa, and Y. Tokura, "Transformation between meron and skyrmion topological spin textures in a chiral magnet," Nature **564**, 95–98 (2018).
[3] B. Göbel, I. Mertig, and O. A. Tretiakov, "Beyond skyrmions: Review and perspectives of alternative magnetic quasiparticles," Phys. Rep. **895**, 1–28 (2021).
[4] H. Ge, X.-Y. Xu, L. Liu, R. Xu, Z.-K. Lin, S.-Y. Yu, M. Bao, J.-H. Jiang, M.-H. Lu, and Y.-F. Chen, "Observation of acoustic skyrmions," Phys. Rev. Lett. **127**, 144502 (2021).
[5] R. D. Muelas-Hurtado, K. Volke-Sepúlveda, J. L. Ealo, F. Nori, M. A. Alonso, K. Y. Bliokh, and E. Brasselet, "Observation of polarization singularities and topological textures in sound waves," Phys. Rev. Lett. **129**, 204301 (2022).
[6] T. Fujita, M. Nakahara, T. Ohmi, and T. Tsuneto, "Textures in rotating superfluid ^{3}He-A," Prog. Theor. Phys. **60**, 671–682 (1978).

[7]Y. M. Bunkov and H. Godfrin, *Topological Defects and the Non-Equilibrium Dynamics of Symmetry Breaking Phase Transitions* (Springer Science+Business Media, 2000), Vol. 549, pp. 325–344.
[8]Y. Shen, Q. Zhang, P. Shi, L. Du, X. Yuan, and A. V. Zayats, "Optical skyrmions and other topological quasiparticles of light," Nat. Photonics **18**, 15–25 (2024).
[9]L. Du, A. Yang, A. V. Zayats, and X. Yuan, "Deep-subwavelength features of photonic skyrmions in a confined electromagnetic field with orbital angular momentum," Nat. Phys. **15**, 650–654 (2019).
[10]R. Gutiérrez-Cuevas and E. Pisanty, "Optical polarization skyrmionic fields in free space," J. Opt. **23**, 024004 (2021).
[11]S. Tsesses, E. Ostrovsky, K. Cohen, B. Gjonaj, N. Lindner, and G. Bartal, "Optical skyrmion lattice in evanescent electromagnetic fields," Science **361**, 993–996 (2018).
[12]X. Lei, A. Yang, P. Shi, Z. Xie, L. Du, A. V. Zayats, and X. Yuan, "Photonic spin lattices: Symmetry constraints for skyrmion and meron topologies," Phys. Rev. Lett. **127**, 237403 (2021).
[13]Q. Zhang, Z. Xie, P. Shi, H. Yang, H. He, L. Du, and X. Yuan, "Optical topological lattices of bloch-type skyrmion and meron topologies," Photonics Res. **10**, 947–957 (2022).
[14]A. Ghosh, S. Yang, Y. Dai, Z. Zhou, T. Wang, C.-B. Huang, and H. Petek, "A topological lattice of plasmonic merons," Applied Physics Reviews **8**, 041413 (2021).
[15]A. Ghosh, S. Yang, Y. Dai, and H. Petek, "The spin texture topology of polygonal plasmon fields," ACS Photonics **10**, 13–23 (2023).
[16]J. Beršky and S. Orlov, "Accelerating airy beams with particle-like polarization topologies and free-space bimeronic lattices," Opt. Lett. **48**, 1168–1171 (2023).
[17]Y. Shen, "Topological bimeronic beams," Opt. Lett. **46**, 3737–3740 (2021).
[18]Y. Shen, C. He, Z. Song, B. Chen, H. He, Y. Ma, J. A. Fells, S. J. Elston, S. M. Morris, M. J. Booth, and A. Forbes, "Topologically controlled multiskyrmions in photonic gradient-index lenses," Phys. Rev. Appl. **21**, 024025 (2024).
[19]A. M. Beckley, T. G. Brown, and M. A. Alonso, "Full poincaré beams," Opt. Express **18**, 10777–10785 (2010).
[20]S. Donati, L. Dominici, G. Dagvadorj, D. Ballarini, M. De Giorgi, A. Bramati, G. Gigli, Y. G. Rubo, M. H. Szymańska, and D. Sanvitto, "Twist of generalized skyrmions and spin vortices in a polariton superfluid," Proc. Natl. Acad. Sci. U. S. A. **113**, 14926–14931 (2016).
[21]S. Gao, F. C. Speirits, F. Castellucci, S. Franke-Arnold, S. M. Barnett, and J. B. Götte, "Paraxial skyrmionic beams," Phys. Rev. A **102**, 053513 (2020).
[22]Y. Shen, E. C. Martínez, and C. Rosales-Guzmán, "Generation of optical skyrmions with tunable topological textures," ACS Photonics **9**, 296–303 (2022).
[23]A. Hansen, J. T. Schultz, and N. P. Bigelow, "Singular atom optics with spinor Bose–Einstein condensates," Optica **3**, 355–361 (2016).
[24]R. D. Ramkhalawon, T. G. Brown, and M. A. Alonso, "Imaging the polarization of a light field," Opt. Express **21**, 4106–4115 (2013).
[25]V. Curcio, L. A. Alemán-Castañeda, T. G. Brown, S. Brasselet, and M. A. Alonso, "Birefringent Fourier filtering for single molecule coordinate and height super-resolution imaging with dithering and orientation," Nat. Commun. **11**, 5307 (2020).
[26]S. K. Pal and P. Senthilkumaran, "Cultivation of lemon fields," Opt. Express **24**, 28008–28013 (2016).
[27]D. Marco, I. Herrera, S. Brasselet, and M. A. Alonso, "Propagation-invariant optical meron lattices," ACS Photonics **11**, 2397 (2024).
[28]R. Fathauer, *Tessellations: Mathematics, Art, and Recreation* (CRC Press, 2020), p. 21.
[29]C. S. Peirce, "A quincuncial projection of the sphere," Am. J. Math. **2**, 394–396 (1879).
[30]O. S. Adams, *Elliptic Functions Applied to Conformal World Maps* (US Government Printing Office, 1925), Vol. 297, pp. 72–78.
[31]L. Lee, "Some conformal projections based on elliptic functions," Geogr. Rev. **55**, 563–580 (1965).
[32]L. Lee, "Conformal projections based on Dixon elliptic functions," Cartographica **13**, 38–66 (1976).
[33]H. A. Schwarz, "Ueber einige abbildungsaufgaben," J. Fur Reine Angew. Math. **70**, 105–120 (1869).
[34]L. Lee, "Conformal projections based on Jacobian elliptic functions," Cartographica **13**, 67–101 (1976).
[35]E. van Fossen Conrad and P. Flajolet, "The Fermat cubic, elliptic functions, continued fractions, and a combinatorial excursion," Sémin. Lothar. Comb. **54**, 1–44 (2006).
[36]I. Freund, "Polarization singularities in optical lattices," Opt. Lett. **29**, 875–877 (2004).
[37]M. Dennis, "Polarization singularities in paraxial vector fields: Morphology and statistics," Opt. Commun. **213**, 201–221 (2002).
[38]C. Maurer, A. Jesacher, S. Fürhapter, S. Bernet, and M. Ritsch-Marte, "Tailoring of arbitrary optical vector beams," New J. Phys. **9**, 78 (2007).
[39]E. Bolduc, N. Bent, E. Santamato, E. Karimi, and R. W. Boyd, "Exact solution to simultaneous intensity and phase encryption with a single phase-only hologram," Opt. Lett. **38**, 3546–3549 (2013).
[40]L. Lee, "Conformal projections of the sphere or parts of the sphere within a circle," Cartographica **13**, 15–37 (1976).
[41]O. S. Adams, *Conformal Projection of the Sphere Within a Square* (US Government Printing Office, 1929), Vol. 4.
[42]J. Cox, "Représentation de la surface entière de la terre dans un triangle équilatéral," Bull. Cl. Sci., Acad. R. Belg. **21**, 66–71 (1936).
[43]D. Sugic, R. Droop, E. Otte, D. Ehrmanntraut, F. Nori, J. Ruostekoski, C. Denz, and M. R. Dennis, "Particle-like topologies in light," Nat. Commun. **12**, 6785 (2021).
[44]W. Lin, N. Mata-Cervera, Y. Ota, Y. Shen, and S. Iwamoto, "Space-time hopfion crystals," arXiv:2406.06096 (2024).
[45]D. Marco and M. A. Alonso, "Optical fields spanning the 4D space of nonparaxial polarization," arXiv:2212.01366 (2022).